IMPROVING STRUCTURAL-INFORMATION RECOVERY IN JOINT MIGRATION INVERSION USING AN IMAGE-BASED REGULARIZATION

C. A. M. Assis and J. Schleicher

email: *js@ime.unicamp.br*

keywords: *Seismic imaging, velocity analysis, joint migration inversion, one-way wave equation*

ABSTRACT

Joint Migration Inversion (JMI) can be formulated to simultaneously estimate parameters of scattering operators associated to the seismic image and of the slowness or velocity model. The inversion strategy can be implemented by alternating updates of each parameter class or in a simultaneous manner. Since JMI is not a well-posed inverse problem, regularization can help to stabilize the problem and/or to select an acceptable subset of the possible solutions according to their predefined desirable characteristics, which are then embedded in the choice of the regularizing function. We propose to take advantage of the structural information available in the inverted image by means of a simple Tikhonov type regularization applied to the tomography part of the JMI method. Tests with two synthetic data sets indicate the effectiveness of the proposed regularization. The methodology developed here is readily applicable to any seismic tomography at practically no additional cost if a migrated image is available.

INTRODUCTION

Joint Migration Inversion (JMI) is an approach to the seismic inverse problem based on scattering and propagation operators (Berkhout, 2014b). In its most simple form, the scattering operator is given by the stacked seismic image. Primarily, it carries information related to the subsurface impedance contrasts at the boundaries between geologic formations. In contrast, the estimated velocities carry information about each layer interval. Therefore, given the nature of the information present in the image and velocity models, it is quite not unusual to think of these quantities as being uncorrelated. However, layer boundaries actually correlate with strong velocity variations. Thus, with additional analytical relations between these quantities, it is possible to make them approximately correlate in the inversion process, for example, by taking the derivative of the velocity profile to transform it into a reflectivity series or by integrating the image to transform it into impedance (see, e.g., Assis et al., 2019).

Establishing relationships between different classes of parameters or different data types is very common in geophysical inverse problems. For example, Gallardo and Meju (2003) propose the cross-gradients constrain which relates the cross-product of the model-parameters gradient to enforce structural similarity in the inversion. Also, imposing structural information from the image to the velocity model has already been proposed using different methodologies. Costa et al. (2008) applied a structurally motivated smoothing constraint in the direction of a potential reflector in slope tomography and showed that this constraint led to geologically more consistent models. Williamson et al. (2011) solved a differential equation to smooth the updated velocity model consistently with structural information.

In the context of JMI, Maciel et al. (2015) applied morphological operators directly to the updated velocity model. Masaya and Verschuur (2018) proposed a regularization for the tomography part of the JMI that relates the image and an approximate image obtained from the velocity model. In this manner,

Masaya and Verschuur (2018) improved the structural information in the velocity model update and not in the velocity directly like Williamson et al. (2011) and Maciel et al. (2015).

Regularization of ill-posed inverse problems is fundamental. It has basically two roles, one being to reduce instability and the other to select solution candidates according to desired characteristics of the solution. These are carried over to the problem by means of the regularization function (Zhdanov, 2015). For example, defining the regularization term as the first derivative of the model parameter penalizes roughness and favors smooth estimates or, in the words of Constable et al. (1987), the simplest model that explains the data.

Inspired by cross-gradients regularization, we investigate a cross-correlation minimization between the image and velocity models in order to make use of the high spatial-frequency information from the image in the velocity updates. We also analyze the inclusion of each parameter's gradient in the regularization function. We demonstrate the effectiveness of the methodologies on two synthetic models. The regularization developed here is very similar to the one of Masaya and Verschuur (2018), but there is no need of an approximate or exact analytical relationship between the parameters. The only assumption needed here is that the events in the image are, to some extent, correlated with velocity contrasts.

REGULARIZING FUNCTIONS

We want to make use of the intrinsic connection between the velocity distribution $v(x,z)$ and the image $R^+(x,z)$, in which x indicates the horizontal coordinate and z is depth. Image R^+ represents the reflection coefficient for incidence from above on a boundary between adjacent layers. It is assumed to be equivalent to the stacked image estimated in most least-squares migration methods.

In the following subsections we define two regularizing functions that use this connection, with focus on using the image information in the velocity or slowness update.

Function I: Correlation of the image and velocity parameters

We define the first regularization function as the zero-lag cross-correlation between velocity and image, i.e.,

$$J_{reg1}(v) = \int_\Omega v(x',z')R^+(x',z')dx'dz' \,, \tag{1}$$

where Ω is the domain of the model parameters. With this regularization function, we try to incorporate the fact that areas of constant velocities have low reflectivity. The kernel of its first derivative with respect to velocity is the image, i.e.,

$$\frac{\partial J_{reg1}}{\partial v} = R^+(x,z)\,. \tag{2}$$

Function II: Velocity and image gradients

We define our second regularization function as the zero-lag cross-correlation between gradients of velocity and image, i.e.,

$$\begin{aligned} J_{reg2}(v) = &\frac{1}{2}\int_\Omega \nabla v(x',z')\cdot\nabla R^+(x',z')dx'dz' \\ &+\frac{1}{4}\int_\Omega v(x',z')\nabla R^+(x',z')\cdot\mathbf{n} - R^+(x',z')\nabla v(x',z')\cdot\mathbf{n}\,dx'dz' \,, \end{aligned} \tag{3}$$

where $\mathbf{n} = (1,1)$. Regularization of the gradients aims at penalizing roughness inside the layers in the inversion. The actually implemented version of regularization function (3) is slightly different. Integration by parts and adoption of homogeneous boundary conditions yields

$$J_{reg2}(v) = \frac{1}{2}\int_\Omega v(x',z')\left[-\nabla^2 R^+(x',z') + \nabla R^+(x',z')\cdot\mathbf{n}\right]dx'dz' \,. \tag{4}$$

Hence, the kernel of this function derivative with respect to velocity is simply

$$\frac{\partial J_{reg2}}{\partial v} = \frac{1}{2}\left[-\nabla^2 R^+(x,z) + \nabla R^+(x,z)\cdot\mathbf{n}\right] \tag{5}$$

Slowness parameterization

To recduce scaling issues in the inverse problem, we parametrized our implementation in terms of the slowness logarithm $\sigma_L = \ln(v_0/v)$, where v_0 denotes some reference velocity (in our implementation, we chose a unit reference velocity). Thus, instead of the derivatives of the regularization functions with respect to v, we need those with respect to σ_L. The chain rule allows us to write

$$\frac{\partial J_{reg}}{\partial \sigma_L} = \frac{\partial J_{reg}}{\partial v}\frac{\partial v}{\partial \sigma_L} = -v\frac{\partial J_{reg}}{\partial v} = -\frac{\partial J_{reg}}{\partial v} v_0 e^{-\sigma_L}\,, \tag{6}$$

where the velocity derivative is given, according to the chosen regularization function, by equation (2) or (5). Our actual implementation uses a normalized version of σ_L varying only in the interval $[-1, 1]$.

INVERSE PROBLEM

Misfit function and forward modelimg

By alternating between imaging and tomography, JMI aims at estimating the reflection coefficient R^+, also interchangeably denominated image, and the slowness parameter σ_L. We search for those values of R^+ and σ_L that minimize the least-squares misfit function

$$E(R^+, \sigma_L) = \frac{1}{2}\frac{\sum_{s=1}^{N_s}\sum_{l=1}^{N_\omega}\|D^-_{sl} - \mathcal{S}_s P^-_{sl}\|_2^2}{\sum_{s=1}^{N_s}\sum_{l=1}^{N_\omega}\|D^-_{sl}\|_2^2} + \lambda J_{reg}\,, \tag{7}$$

where s is the shot index and N_s is the number of shots, l is the angular-frequency index and N_ω is the number of angular frequencies. Moreover, D^-_{sl} is the upgoing observed data, P^-_{sl} is the upgoing modeled data, $\mathcal{S}_s$ is a operator that samples the upgoing wavefield at the receiver positions, λ is a Lagrangian regularization parameter, and $\|.\|_2^2$ denotes the L^2 norm squared over the receivers.

The recursive integral representation of the modeled downgoing P^+ and upgoing P^- wavefields are (Berkhout, 2014b)

$$P^+_{j+1}(x', z_{n+1}, \omega) = \hat{\mathcal{G}}^+(x', z_{n+1}, \omega; x, z_n)\left(R^- P^-_j + T^+ P^+_{j+1} + \Delta z S^+\right)(x, z_n, \omega)\,, \tag{8}$$

$$P^-_{j+1}(x', z_{n-1}, \omega) = \hat{\mathcal{G}}^-(x', z_{n-1}, \omega; x, z_n)\left(R^+ P^+_{j+1} + T^- P^-_{j+1}\right)(x, z_n, \omega)\,, \tag{9}$$

where $\hat{\mathcal{G}}^+(x', z_{n+1}, \omega; x, z_n)$ and $\hat{\mathcal{G}}^-(x', z_{n-1}, \omega; x, z_n)$ are the upgoing and downgoing Green's operators. They represent integrals over the lateral coordinate and perform extrapolation from a boundary at depth level z_n to $z_{n\pm1}$, respectively. They can be implemented using any one-way wave propagator. Moreover, the subscript j is related to the scattering order, z_n is the nth boundary, $z_{n\pm1} = z_n \pm \Delta z$, $T^\pm$ are angle-independent transmission coefficients, $R^\pm$ are the angle-independent reflection coefficients and S^+ is the downgong source. For a detailed explanation of these equations see Berkhout (2014a).

The zero-order terms are the single-scattering wavefields given by the Born approximation, i.e.,

$$P^+_0(x', z_{n+1}, \omega) = \hat{\mathcal{G}}^+(x', z_{n+1}, \omega; x, z_n)\left(T^+ P^+_0 + \Delta z S^+\right)(x, z_n, \omega)\,, \tag{10}$$

$$P^-_0(x', z_{n-1}, \omega) = \hat{\mathcal{G}}^-(x', z_{n-1}, \omega; x, z_n)\left(R^+ P^+_0 + T^- P^-_0\right)(x, z_n, \omega)\,. \tag{11}$$

Partial derivatives

In this section we omit the subscript related to the scattering order. In the forward modeling implmentation we keep the upgoing wavefield the same between iterations.

Using the Lagrangian-multiplier method, we derive the gradients of the misfit function, equation (7), with respect to the model parameters. These gradients are required by the steepest-descent method. Considering only variations of the upgoing wavefield, i.e., the so-called receiver side, and neglecting resulting variations in the downgoing wavefield, the gradient of the misfit function with respect to R^+ is

$$\frac{\partial E}{\partial R^+}(z) = -\,\boldsymbol{Re}\left\{\sum_{s=1}^{N_s}\sum_{l=1}^{N_\omega}\left[P^+_{sl}(z)\right]^*\Lambda^-(z)\right\}\,, \tag{12}$$

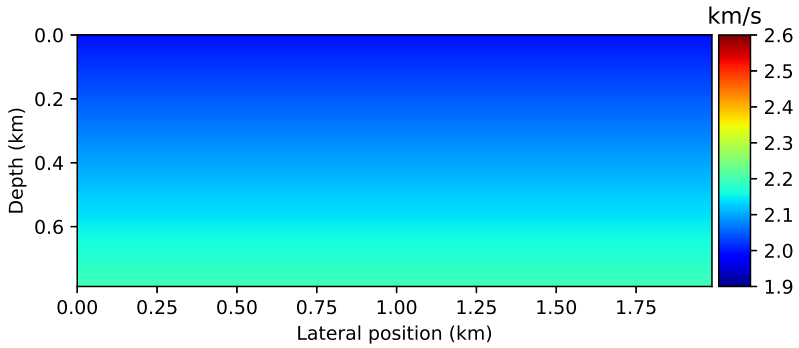

Figure 1: Lens model: (a) Initial velocity model for inversion.

where $\boldsymbol{Re}$ is the real-part operator and the asterisk denotes complex conjugate. Here, we exhibit only the dependence on the depth coordinate to simplify notation. Additionally, we have multiplied the right-hand side of equation (12) by -1 to obtain as descent direction.

The adjoint wavefield Λ^- is given by

$$\Lambda^-_{sl}(x', z_{n+1}, \omega) = \hat{\mathcal{G}}^+(x', z_{n+1}, \omega; x, z_n) \left[\frac{1}{T^-} \Lambda^-_{sl} - \Delta z \mathcal{S}^t_s \left(D^-_{sl} - \mathcal{S}_s P^-_{sl} \right) \right] (x, z_n, \omega) \,, \tag{13}$$

where the superscript t denotes transpose. Here, we have replace the adjoint of the transmission operator division by inverse of the transmission coefficient. We believe that this should help to balance the amplitude of deep reflection coefficients relatively to the shallow ones.

The corresponding gradient of E with respect to σ_L is

$$\frac{\partial E}{\partial \sigma_L}(z) = - \boldsymbol{Re} \left\{ \sum_{s=1}^{N_s} \sum_{l=1}^{N_\omega} \left[i \hat{\mathcal{H}}_1^{-1} \frac{\omega^2}{v^3} \frac{\partial v}{\partial \sigma_L} P^-_{sl} \right] \left[\Lambda^-_{sl}(z) \right]^* \right\} - \lambda \frac{\partial J_{reg}}{\partial \sigma_L}(z) \,, \tag{14}$$

where $\hat{\mathcal{H}}_1$ is the square-root operator of the one-way wave equation (see, e.g., Grimbergen et al., 1998), defined as

$$\hat{\mathcal{H}}_1 = \left[\frac{\partial^2}{\partial x^2} + \frac{\omega^2}{v^2} \right]^{1/2} . \tag{15}$$

The step-length for each parameter update is calculated by a least-squares fit between the present data residual and the perturbed wavefieled calculated using the linearized forward upgoing equation. Update directions are normalized by the squared magnitude of the factor multiplying the adjoint wavefields and stacked over shots and frequencies. This rough approximation of the inverse Hessian is equivalent to the deconvolution imaging condition.

The described approach has a few limitations. A drawback of the decoupling into up and downgoing wavefields is the absence of horizontally propagating waves (Ursin et al., 2012). Moreover, we consider a constant density model, the Green's functions are implemented for a locally homogeneous velocity model as discussed by Thorbecke et al. (2004), and the scattering operators are all considered angle independent.

NUMERICAL TESTS

We demonstrate the use of the proposed regularization functions with the help of two numerical examples using synthetic data from two velocity models of different geological complexity. The first model is a variation of the model used for similar purposes in Masaya and Verschuur (2018). It contains a lens shaped velocity anomaly and fine layering at the bottom. The second model is the modified Marmousi2 model of Pan et al. (2018). The same algorithm using a multiscale approach was used for modeling and inversion. In both tests, we used a Ricker wavelet with 20 Hz peak frequency.

The inversion works in frequency stages. Whenever the misfit function change was less than 1% as compared to the previous iteration, or if a maximum number of 20 iteration was reached, our procedure

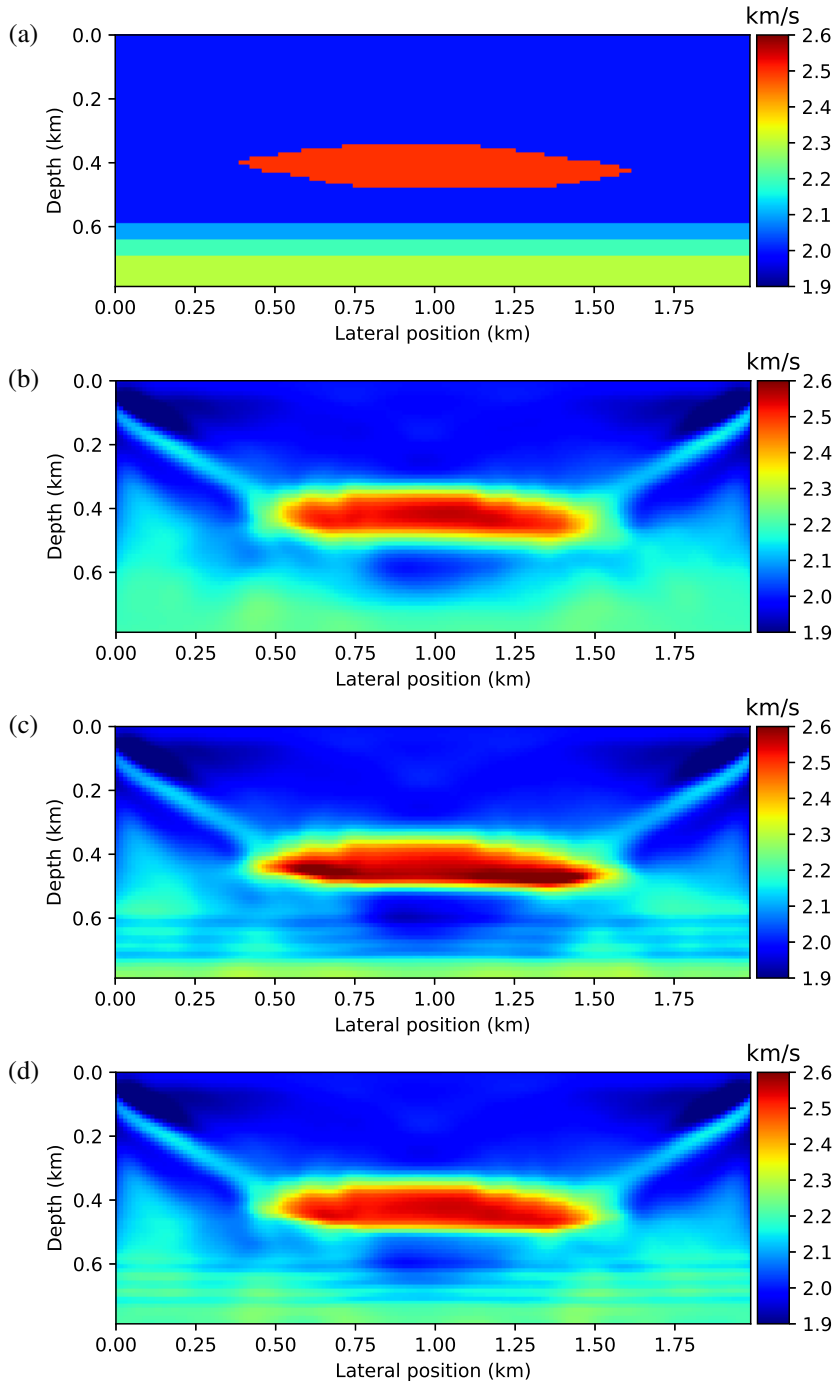

Figure 2: Lens model: (a) Exact velocity model; (b) Velocity model from tomography without regularization; (c) Velocity model from tomography with regularization I; (d) Velocity model from tomography with regularization II.

initiated a new frequency stage. We fixed the minimum frequency at the first sample after 0 Hz. The initial value of the regularization parameter was defined as the ratio between the maximum values of the model-parameter update and the regularization term. This value was then multiplied by a scaling factor which was doubled at each new stage.

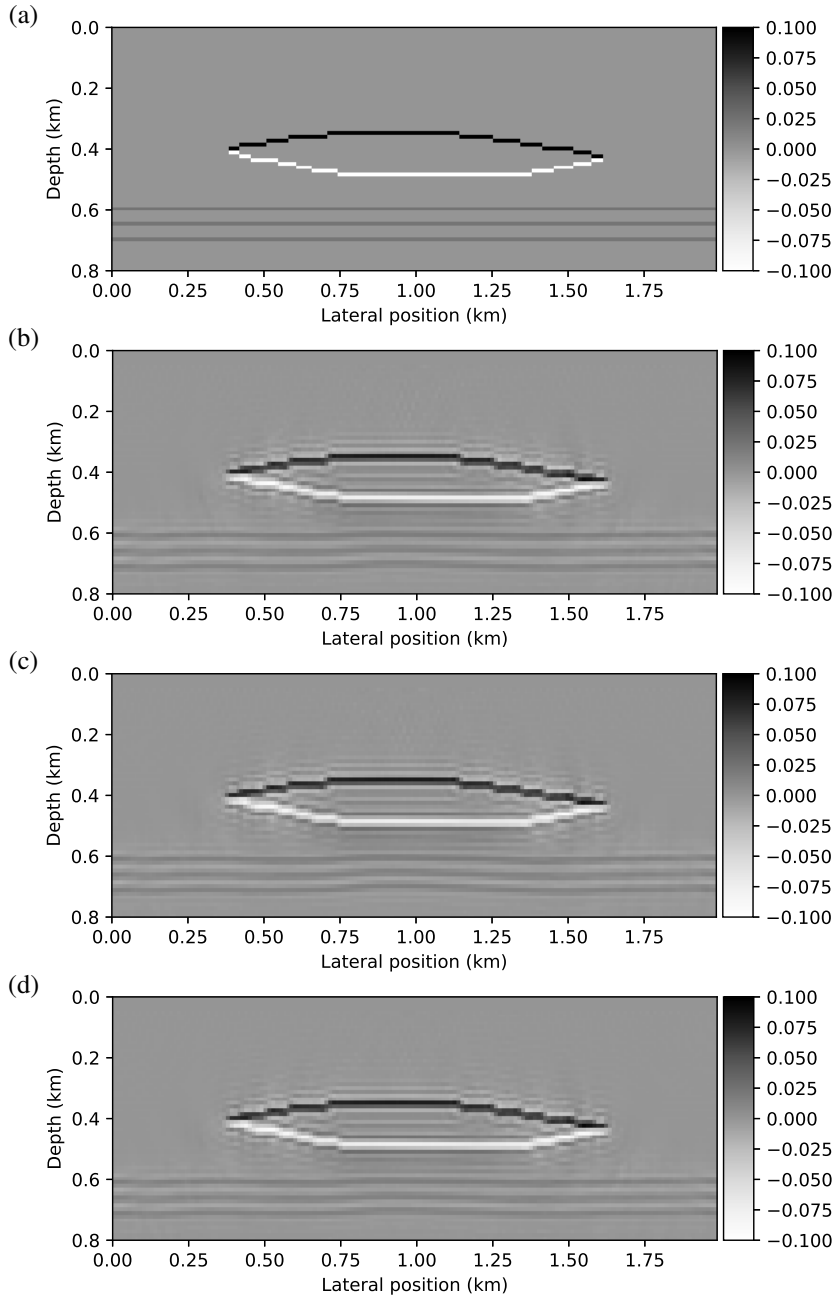

Figure 3: Lens model: (a) Exact reflectivity image; (b) Reflectivity image from tomography without regularization; (c) Reflectivity image from tomography with regularization I; (d) Reflectivity image from tomography with regularization II.

Lens model

For the test in this model, we divided the frequency stages into six intervals, with the first maximum frequency at 15 Hz and increments of 5 Hz. The initial velocity model was a linear gradient starting at 2000 m/s at the top of the model and ending at 2200 m/s at its bottom (see Figure 1). The starting regularization parameter scaling factor was 0.025. Figure 2a shows the exact velocity model used in this example.

Figure parts 2b, c and d show the inverted models with no regularization and our two proposed regular-

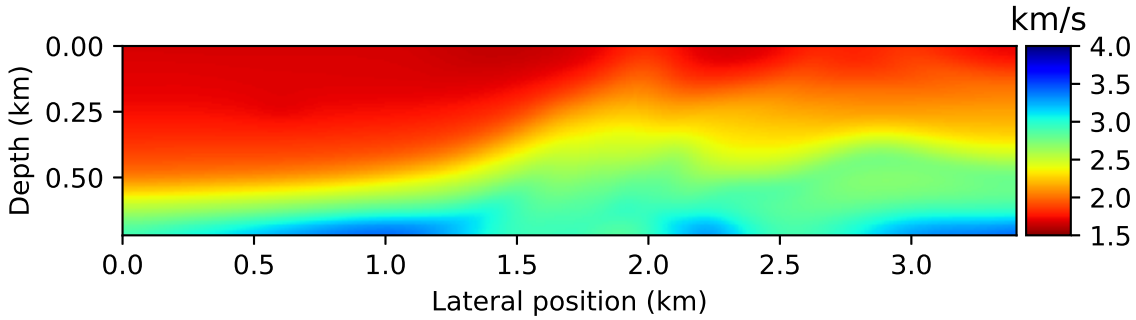

Figure 4: Marmousi2 model: Initial velocity model.

izations, respectively. The estimated velocity model without regularization (Figure 2b) is already a more or less acceptable result. Regularization I improves the resolution in the velocity model, as can be seen from the lens shape, particularly at the fine edges, and the fine layering below (Figure 2c. The resolution of the velocity model obtained with regularization II (Figure 2d) is better than with no regularization but worse than with regularization I.

The corresponding images to these velocity models are depicted in Figure 3. Figure 3a shows the exact reflectivity image. We observe that the image obtained without regularization is already quite good (Figure 3b). Note, however, that the horizontal reflectors at the bottom of the image are positioned slightly below their correct depth. We have seen in Figure 2 that regularization I improves the quality of the velocity model. The consequence of this improvement in the image (Figure 3c) is the slight pull-up of the horizontal reflectors below the lens to their correct depths. To the sides of the lens, reduced illumination leads to unsufficient data even with regularization. The image obtained with regularization II (Figure 3d) is better than with no regularization but worse than with regularization I, in full correspondence to the observations regarding the velocity models. While the reflector positions below the lense are slightly corrected as compared to the image without regularization, they are not as good positioned as in the image with regularization I.

Marmousi2 model

For this experiment, we divided the frequency stages into four intervals, with the first maximum frequency at 10 Hz and an increment of 10 Hz. The initial velocity model was a strongly smoothed version of the exact model (see Figure 4). Figure 5a shows the exact velocity model. The starting regularization parameter scaling factor was 0.05.

The estimated velocity model without regularization already provides a reasonable representation of the true velocity distribution (Figure 5b). Many details were introduced in the velocity model that are absent in the initial velocity model. Regularization I enhanced the details in the velocity model, notably in the lateral intervals between 0 and 1.5 km and from 2.1 km until the right end (Figure 5c). Regularization II led to a slightly smoother verion of the velocity model (Figure 5d).

Figure 6a shows the exact reflectivity image. The estimated image without regularization already provides a reasonable representation of the geology (Figures 6b). The most prominent reflectors are well imaged throughout the model. In the images obtained with regularization (Figures 6c,d), it is hard to spot any significant differences. As a subtle difference, the deepest reflector on the right-hand side of the image seems to be slightly better positioned in the image obtained with regularization I (Figure 6c) than in the other two inverted images.

CONCLUSION

We have discussed a simple regularization function for the tomography part of JMI to enhance the structural information in the velocity updates. It is based on the cross-correlation between the velocity and the image information. We have tested two versions, regularization I, using the velocity and image themselves, and regularization II, using the respective gradients. In our numerical tests, we increased the regularization

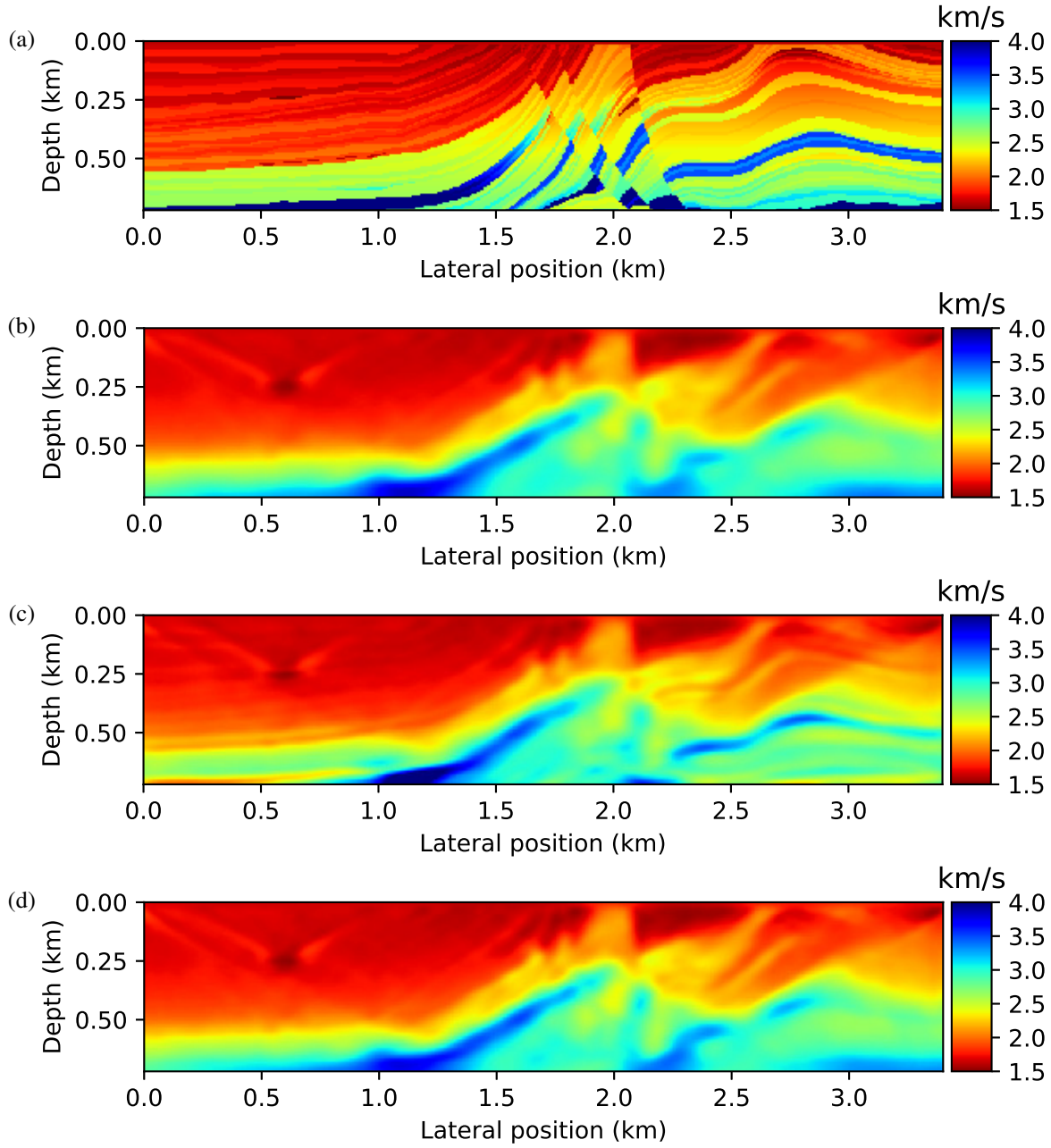

Figure 5: Marmousi2 model: (a) Exact velocity model; (b) Velocity model from tomography without regularization; (c) Velocity model from tomography with regularization I; (d) Velocity model from tomography with regularization II.

parameter at each new frequency stage with the aim of slowly imposing the structural information from the image onto the velocity.

Our numerical experiments on a simple lens model and the modified Marmousi2 model demonstrated that regularization I helped to increase the resolution in the resulting velocity model, which led to a slightly improved image. Regularization II, on the other hand, helped to keep an overall smoother velocity model.

Generally speaking, using identical inversion parameterization, regularization I was qualitatively more effective than regularization II. The extra computational cost is negligible in both approaches and the methodology studied here can be applied in any tomographic technique if a seismic image is available.

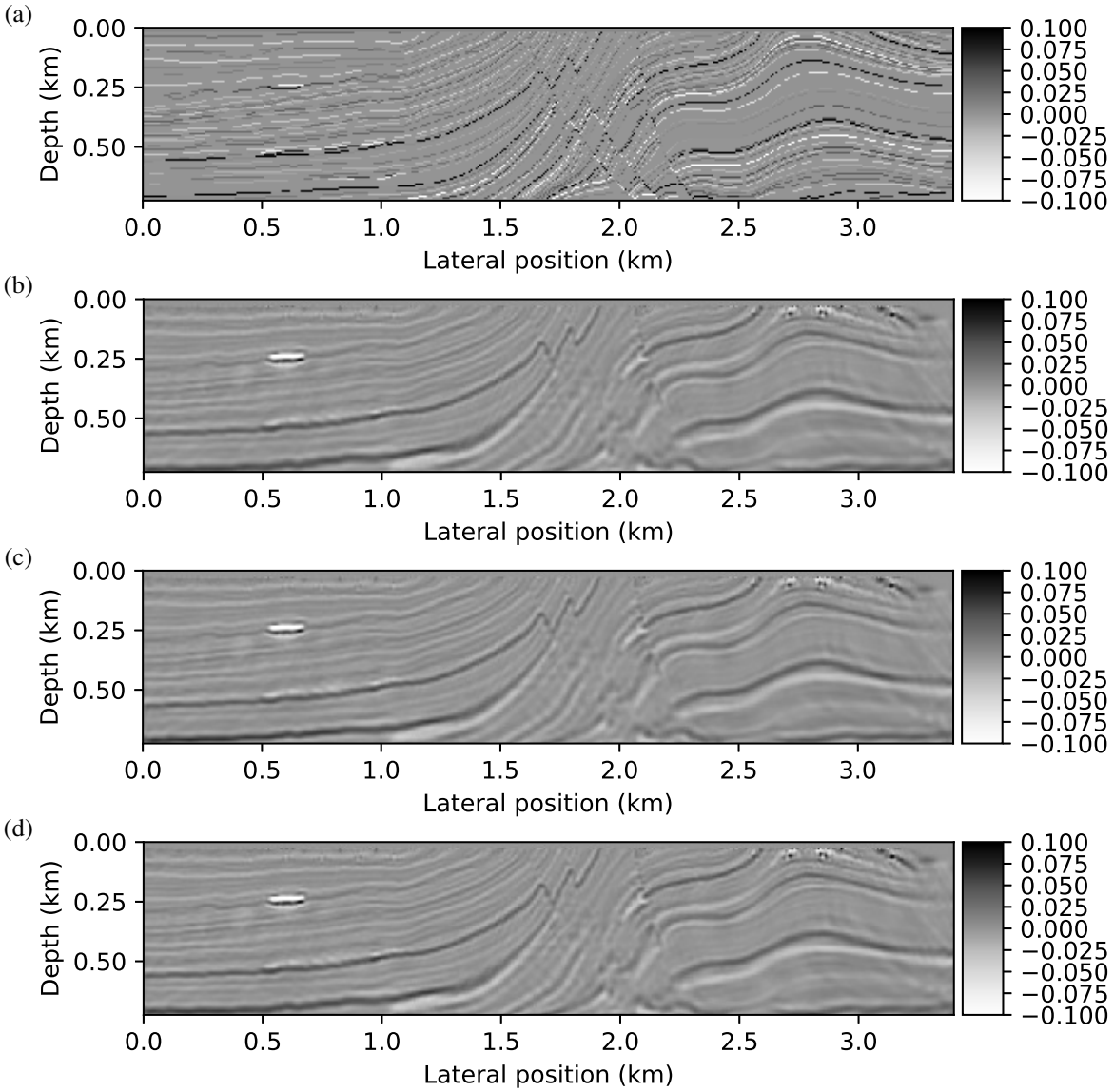

Figure 6: Marmousi2 model: (a) Exact reflectivity image; (b) Reflectivity image from tomography without regularization; (c) Reflectivity image from tomography with regularization I; (d) Reflectivity image from tomography with regularization II.

ACKNOWLEDGMENTS

The authors are grateful to Peter Américo Machado and João Cândido Magalhães for valuable discussions, and to Prof. Dr. Eric Verschuur (Delft University of Technology) who kindly provided computer programs with basic JMI algorithms at the beginning of this work. This study was funded by Petrobras, ANP, PRH-PB15, and PRH-PB230. The first author also thanks the exchange program scholarship provided by Capes/CNPq/DAAD process no. {88887.161391/2017-00}. Additional support for the authors was provided by CAPES, CNPq, and the sponsors of the *Wave Inversion Technology (WIT) Consortium*.

REFERENCES

Assis, C. A. M., Santos, H. B., and Schleicher, J. (2019). Colored and linear inversions to relative acoustic impedance. *Geophysics*, 84(2):N15–N27.

Berkhout, A. G. (2014a). Review Paper: An outlook on the future of seismic imaging, Part I: forward and reverse modelling. *Geophysical Prospecting*, 62(5):911–930.

Berkhout, A. G. (2014b). Review paper: An outlook on the future of seismic imaging, Part III: Joint migration inversion. *Geophysical Prospecting*, 62(5):950–971.

Constable, S. C., Parker, R. L., and Constable, C. G. (1987). Occam's inversion: A practical algorithm for generating smooth models from electromagnetic sounding data. *Geophysics*, 52(3):289–300.

Costa, J. C., da Silva, F. J. C., Gomes, E. N. S., Schleicher, J., Melo, L. A. V., and Amazonas, D. (2008). Regularization in slope tomography. *Geophysics*, 73(5):VE39–VE47.

Gallardo, L. A. and Meju, M. A. (2003). Characterization of heterogeneous near-surface materials by joint 2D inversion of DC resistivity and seismic data. *Geophysical Research Letters*, 30(13):1658–1661.

Grimbergen, J. L. T., Dessing, F. J., and Wapenaar, K. (1998). Modal expansion of one-way operators in laterally varying media. *Geophysics*, 63(3):995–1005.

Maciel, J., Costa, J., and Verschuur, D. (2015). Enhancing resolution in imaging-based velocity estimation using morphological operators. In *SEG Technical Program Expanded Abstracts 2015*, pages 5228–5232. Society of Exploration Geophysicists.

Masaya, S. and Verschuur, D. J. E. (2018). Iterative reflectivity-constrained velocity estimation for seismic imaging. *Geophysical Journal International*, 214(1):1–13.

Pan, W., Geng, Y., and Innanen, K. A. (2018). Interparameter trade-off quantification and reduction in isotropic-elastic full-waveform inversion: synthetic experiments and hussar land data set application. *Geophysical Journal International*, 213(2):1305–1333.

Thorbecke, J. W., Wapenaar, K., and Swinnen, G. (2004). Design of one-way wavefield extrapolation operators, using smooth functions in WLSQ optimization. *Geophysics*, 69(4):1037–1045.

Ursin, B., Pedersen, Ø., and Arntsen, B. (2012). Flux-normalized wavefield decomposition and migration of seismic data. *Geophysics*, 77(3):S83–S92.

Williamson, P., Atle, A., Fei, W., and Hale, D. (2011). Regularization of wave-equation migration velocity analysis by structure-oriented smoothing. In *SEG Technical Program Expanded Abstracts 2011*, pages 3877–3881. Society of Exploration Geophysicists.

Zhdanov, M. S. (2015). Ill-posed problems and the methods of their solution. In *Inverse Theory and Applications in Geophysics*, pages 33–61. Elsevier.